ANTIOXIDANTS & REDOX SIGNALING
Volume 16, Number 10, 2012

DOI: 10.1089/ars.2011.4221

Production of H_2O_2 in the Endoplasmic Reticulum Promotes *In Vivo* Disulfide Bond Formation

Éva Margittai,[1] Péter Löw,[2] Ibolya Stiller,[1] Alessandra Greco,[3] Jose Manuel Garcia-Manteiga,[4,5] Niccolo Pengo,[4,5] Angelo Benedetti,[3] Roberto Sitia,[4,5] and Gábor Bánhegyi[1]

Abstract

Aims: Oxidative protein folding in the luminal compartment of endoplasmic reticulum (ER) is thought to be accompanied by the generation of H_2O_2, as side-product of disulfide bond formation. We aimed to examine the role of H_2O_2 produced in the lumen, which on one hand can lead to redox imbalance and hence can contribute to ER stress caused by overproduction of secretory proteins; on the other hand, as an excellent electron acceptor, H_2O_2 might serve as an additional pro-oxidant in physiological oxidative folding. ***Results:*** Stimulation of H_2O_2 production in the hepatic ER resulted in a decrease in microsomal GSH and protein-thiol contents and in a redox shift of certain luminal oxidoreductases in mice. The oxidative effect, accompanied by moderate signs of ER stress and reversible dilation of ER cisternae, was prevented by concomitant reducing treatment. The imbalance also affected the redox state of pyridine nucleotides in the ER. Antibody producing cells artificially engineered with powerful luminal H_2O_2 eliminating system showed diminished secretion of mature antibody polymers, while incomplete antibody monomers/dimers were accumulated and/or secreted. ***Innovation:*** Evidence are provided by using *in vivo* models that hydrogen peroxide can promote disulfide bond formation in the ER. ***Conclusion:*** The results indicate that local H_2O_2 production promotes, while quenching of H_2O_2 impairs disulfide formation. The contribution of H_2O_2 to disulfide bond formation previously observed *in vitro* can be also shown in cellular and *in vivo* systems. *Antioxid. Redox Signal.* 16, 1088–1099.

Introduction

Disulfide bond formation in the endoplasmic reticulum (ER) by the sulfhydryl oxidase ER oxidoreductin 1 (Ero1) family is thought to be accompanied by the formation of hydrogen peroxide (1, 12, 16, 36). Since secretory cells can make substantial amounts of proteins that contain disulfide bonds, the production of this reactive oxygen species could have potentially dangerous consequences (22). However, H_2O_2 is not only a harmful by-product leading to oxidative stress, but also a possibly useful electron acceptor that can serve the formation of disulfide bonds from cysteine thiols via a sulfenic acid intermediate (5). A recent *in vitro* study demonstrated that H_2O_2 added directly or generated enzymatically was able to promote the oxidative folding of a model substrate, resulting in the efficient formation of a natively folded protein containing proper disulfide bonds. H_2O_2 also oxidizes the active site of protein disulfide isomerase (PDI) and less efficiently GSH (18). Hence it is possible that H_2O_2 generated either by Ero1 during disulfide bond formation or by other ER flavoproteins, can be utilized in turn for the formation of further disulfide bonds (5, 24). The experiments demonstrating the role of peroxiredoxin 4 (PRDX4) in hydrogen peroxide-dependent disulfide bond formation (35,39) further strengthen this view.

Cells derived from mice carrying gene trap mutations in both Ero1α and Ero1β genes proved to be hypersensitive to

Innovation

Hydrogen peroxide was long thought to be a harmful byproduct of oxidative protein folding. Currently, however, different pathways were hypothesized to take a role in the recycling of H_2O_2 to disulfide bond formation. Here, evidence is provided by using *in vivo* models that hydrogen peroxide can promote disulfide bond formation in the ER.

[1]Department of Medical Chemistry, Molecular Biology and Pathobiochemistry, Semmelweis University, Budapest, Hungary.
[2]Department of Anatomy, Cell and Developmental Biology, Loránd Eötvös University, Budapest, Hungary.
[3]Department of Pathophysiology, Experimental Medicine and Public Health, University of Siena, Siena, Italy.
[4]Universita' Vita-Salute San Raffaele, Milano, Italy.
[5]Division of Genetics and Cell Biology, San Raffaele Scientific Institute, Milano, Italy.

depletion of PRDX4. A possible explanation for this unexpected phenomenon is that PRDX4 can substitute for Ero1 in disulfide bond formation. Indeed, depletion of PRDX4 exacerbated the modest defects in disulfide formation seen in the Ero1α–Ero1β double knockout cells (39). The role of PRDX4 as a hydrogen peroxide dependent disulfide catalyst has been confirmed by an independent *in vitro* study showing the rapid oxidation of PRDX4 by hydrogen peroxide and a consecutive relatively slower transfer of its disulfide to PDI family proteins (35). In accordance with these observations, accumulation of high molecular weight IgM complexes was detected in lymphocytes isolated from PRDX4 knockout mice and differentiated to plasma cells (4).

In wild-type cells, the cooperation between Ero1s and PRDX4 on one hand improves the efficacy of oxidative protein folding by generating two disulfide bonds at the expense of one molecule of oxygen; on the other hand, it would solve the problem of hydrogen peroxide toxicity. However, under the experimental conditions applied by Zito and co-workers (39), hydrogen peroxide sources other than Ero1s should be supposed. The identification of these sources requires further studies.

PRDX4 is presumably not a single candidate as PDI oxidant. A recent study showed that two human glutathione peroxidases (GPx7 and GPx8) are ER-resident PDI peroxidases. They were able to catalyze an efficient protein refolding in the presence of PDI and peroxide. They were shown to interact with Ero1α, suggesting that they can represent a novel pathway for the productive reutilization of hydrogen peroxide produced by Ero1s during disulfide bond formation (28).

The aim of the present study was to demonstrate *in vivo* the role of hydrogen peroxide in disulfide bond formation. To this end, two experimental approaches were used. First, ER-targeted hydrogen peroxide production was provoked in mice, which express an ER membrane flavoprotein gulonolactone oxidase. The enzyme is responsible for the last step of ascorbate synthesis, and the *in vivo* administration of its substrate gulonolactone results in ER luminal ascorbate and—as a by-product—hydrogen peroxide formation (20, 31). In our second model, ER luminal hydrogen peroxide was downregulated by the ER-targeted overexpression of catalase in cellular models where disulfide bond formation is inevitable for proper cellular function. The results confirm and extend the notion that ER luminal hydrogen peroxide can be efficiently reutilized in the electron transfer chain of oxidative protein folding.

Results

ER-targeted hydrogen peroxide production promotes local thiol oxidation

In a set of *in vivo* experiments, the effect of the ER luminal hydrogen peroxide formation on protein thiol oxidation was studied in the liver of mice. To provoke an oxidative folding-independent hydrogen peroxide production in the ER lumen, gulonolactone was administered intraperitoneally. Gulonolactone oxidase metabolizes gulonolactone to ascorbate with the concomitant production of hydrogen peroxide. In accordance with its predicted membrane topology, the catalytic site is positioned in the lumen, thus the enzyme produces hydrogen peroxide (and ascorbate) intraluminally. The presumed effect on glutathione or protein thiol oxidation was mitigated by the coadministration of dithiothreitol (DTT).

Acute and chronic effects of gulonolactone were investigated. The effective dose of gulonolactone was established in preliminary experiments, which showed that 3.5 mg/kg (approx. 20 m*M*/kg) body weight gulonolactone was necessary to obtain a well-measurable stimulation of ascorbate production (Supplementary Fig. S1; supplementary data are available online at www.liebertonline.com/ars). Thus, this dose was used in all of the further experiments. A single intraperitoneal dose of gulonolactone resulted in the swelling of the liver at 30 min with significant increase in liver weights (Fig. 1A). Electron microscopy revealed a dramatic dilation of ER cisternae in the liver, while mitochondrial and nuclear structures (Supplementary Fig. S2) looked intact in the 30-min samples. DTT treatment did not cause significant change in liver weight, though a slight, not significant decrease was observed in accordance with the ultrastructural analysis showing shrunken ER cisternae. DTT coadministration with gulonolactone decreased liver swelling and prevented the altered ER morphology (Figs. 1A and S2). The alterations caused by gulonolactone treatment were completely reversible; the 12-h samples were indistinguishable from the controls (Fig. 1B).

The preventive effect of DTT was not due to the inhibition of gulonolactone oxidase. Gulonolactone addition produced a significant increase in hepatic ascorbate content (expressed as micromoles/liver; concentration would have been misleading due to the swelling), which was not affected by DTT coadministration (Fig. 1A). After 12 hours, the ascorbate level returned to the control value, presumably due to the complete consumption of the added gulonolactone and/or the excretion of gulonolactone and ascorbate (Fig. 1B).

To prove that liver swelling and altered ER morphology were indeed due to the metabolism of gulonolactone (and not to its osmotic or other effect), the treatment was also performed in guinea pigs who lack gulonolactone oxidase activity. As it was expected, gulonolactone administration did not increase hepatic ascorbate levels; moreover, liver swelling and the morphological changes were not observed in guinea pigs (Fig. 1C).

Hydrogen peroxide elimination usually occurs at the expense of NADPH as electron donor in cellular compartments other than the ER. Thus, although ER luminal hydrogen peroxide metabolizing pathways have not been fully understood, we wanted to further characterize the effects of ER-targeted hydrogen peroxide generation on the redox conditions in the lumen of the organelle. The redox state of luminal pyridine nucleotides was shifted towards oxidized direction, as it was estimated by measuring microsomal cortisone–cortisol interconversion (Fig. 2A). This reaction is catalyzed by the luminal enzyme 11β-hydroxysteroid dehydrogenase type 1 (11βHSD1) (2). The reaction is reversible and its direction depends on the availability of reduced and oxidized pyridine nucleotides (*i.e.*, on the [NADPH]/[$NADP^+$] ratio) (10). We observed a marked decrease in cortisol production from cortisone in liver microsomes from gulonolactone-treated mice (Fig. 2A, left panel), while cortisone generation from cortisol was increased (Fig. 2A, right panel). DTT treatment did not change the interconversion and failed to prevent the effects of gulonolactone administration (Fig. 2A). The observed changes were not due to the altered expression of either 11βHSD1 or the main ER luminal NADPH-producing enzyme hexose-6-phosphate dehydrogenase (Fig. 2B) (34). We excluded the

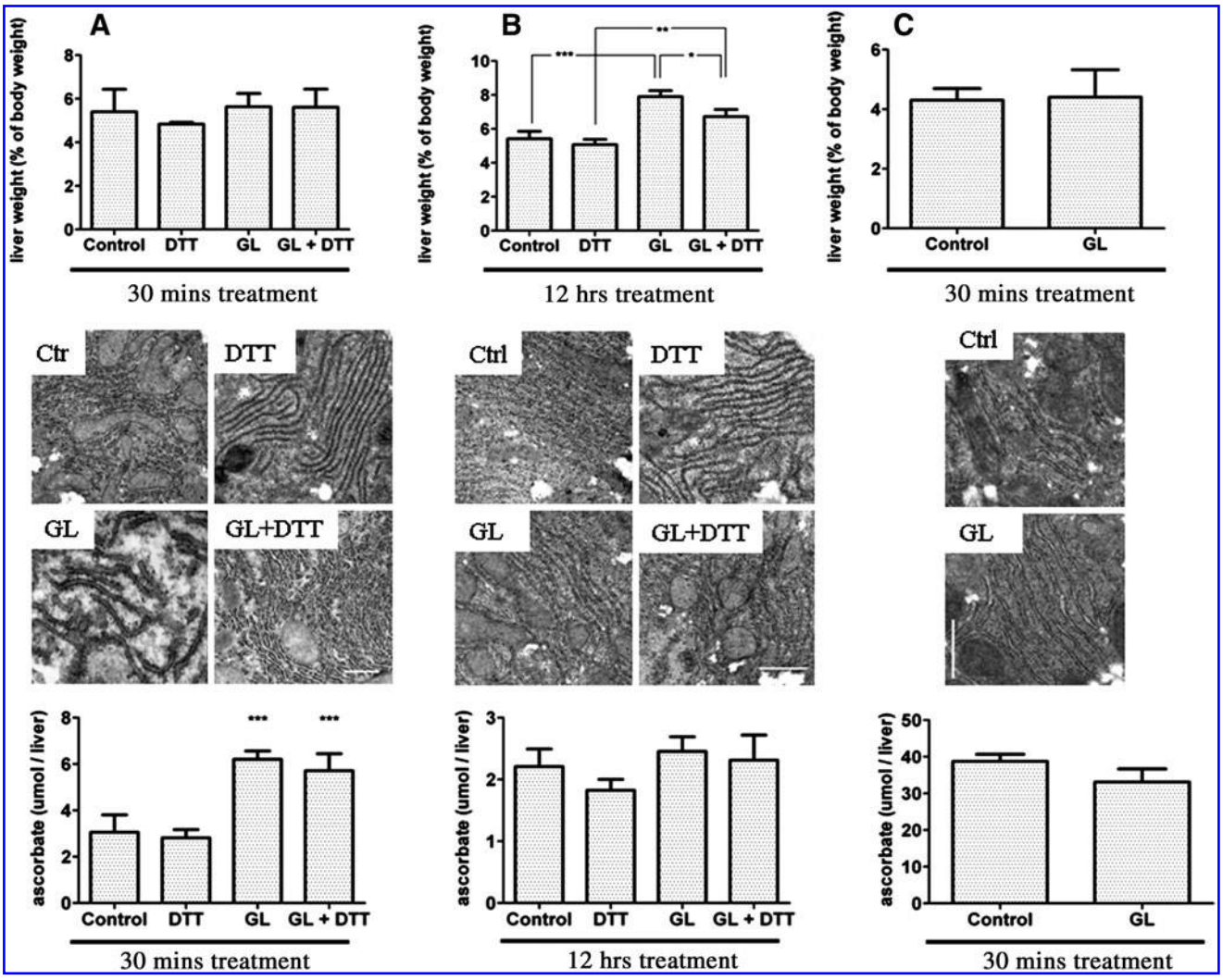

FIG. 1. H_2O_2 overproduction in the ER causes morphological alterations in liver structure reversible by reductant treatment. Mice treated with gulonolactone (GL), dithiothreitol (DTT), or both for 30 min **(A)** or 12 h **(B)** were sacrificed and their livers were removed and analyzed. **(A)** Application of GL resulted in liver swelling after 30 min of the treatment, which was balanced by the coadministration of DTT *(upper panel)*. Electron microscopy *(middle panel)* revealed an altered ultrastructure of ER with dilated cisternae, while mitochondria and nuclear structures remained intact. Parallel DTT treatment reversed the effect of GL also on the ultrastructural level, while DTT alone caused slight shrinkage of ER. Activity of gulonolactone oxidase was assessed by detecting the endproduct—ascorbate—of the enzymatic reaction in total liver homogenates *(lower panel)*. Intraperitoneal addition of GL highly elevated the ascorbate content of the liver, which was not prevented by DTT. **(B)** Morphological changes of liver were completely recovered 12 h after treatment with the above enumerated agents, both at macroscopic and microscopic levels, in accordance with the normalized hepatic ascorbate content in chronically treated mice. **(C)** Liver weights and morphology remained unaltered in guinea pigs treated with GL for 30 mins. Results are expressed as mean ± S.D., $n = 4$–6, $^{***}p < 0.001$, $^{**}p < 0.01$, $^{*}p < 0.05$, bar = 1 μm. Representative images of electron microscopy are shown.

direct effect of gulonolactone on these enzymes: in microsomal measurements gulonolactone up to 10 m*M* concentration did not cause any inhibition (Fig. 2C). The alterations in pyridine nucleotide pool were seen only in the 30-min samples and not in the chronically- treated mice (Fig. 2A, middle panel). In accordance with these results, addition of hydrogen peroxide to liver microsomes resulted in a prompt decrease of the fluorescent signal of reduced pyridine nucleotides (Fig. 2D) indicating a direct oxidizing effect of H_2O_2 on the NADPH/NADH pool.

The redox state of the thiol–disulfide system was also changed in 30-min treated animals. In accordance with our previous results (3, 25, 31), luminally produced H_2O_2 preferentially oxidizes microsomal glutathione. Gulonolactone-treated mice presented a marked decrease in microsomal GSH content, while GSSG content remained unaffected (Fig. 3A). DTT coadministration could not reverse the effect. At the same time, total hepatic GSH content, measured in liver homogenates, was only moderately decreased (Fig. 3B). The alteration of glutathione levels were reversible; 12 h after the treatment glutathione levels returned to the control values both in microsomal fractions (Fig. 3C) and in the homogenates (Fig. 3D).

Here we found that microsomal protein thiol levels also decreased upon gulonolactone addition; DTT reversed the effect (Fig. 4A). A decrease of protein thiol level in total liver

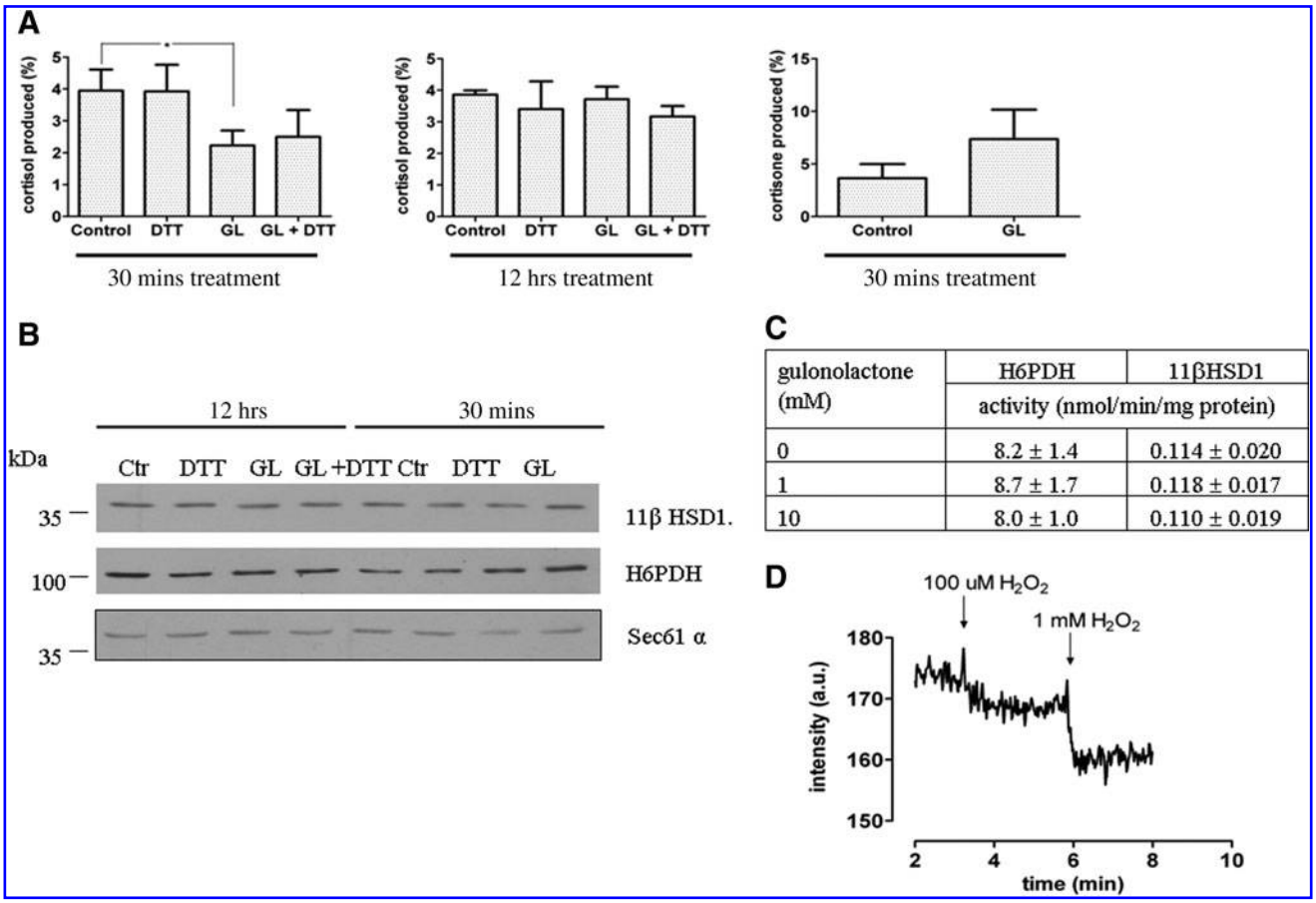

FIG. 2. Luminal hydrogen peroxide oxidizes the ER pyridine nucleotide pool. Mice treated with gulonolactone (GL), dithiothreitol (DTT), or both (GL + DTT) for 30 min or 12 h were sacrificed, and liver microsomes were isolated to analyze the redox state of luminal pyridine nucleotide pool. **(A)** Redox state of pyridine nucleotides was estimated by measuring the cortisone-to-cortisol (*left and middle panels*) or the cortisol-to-cortisone (*right panel*) interconversion and was found to be significantly less reduced in animals treated with GL. Concomitant DTT addition did not protect against this effect. The conversion was expressed as the percentage of added cortisone or cortisol, mean ± S.D., $n = 4$, $^*p < 0.05$. **(B)** Immunoblotting of enzymes responsible for the modulation of intraluminal [NADPH]/[$NADP^+$] pool, [*i.e.* 11β-hydroxysteroid dehydrogenase type 1 (11βHSD1)] and hexose-6-phosphate dehydrogenase (H6PDH) revealed an unaltered expression. Sec61α was also detected as a loading control. **(C)** Gulonolactone up to 10 m*M* concentration was not inhibitory on 11βHSD1 and H6PDH activities in liver microsomes from untreated control mice. Activities were detected on the basis of fluorimetric measurement of NADPH formation. Results are expressed as means ± S.D., $n = 4$. **(D)** The direct oxidizing effect of 100 μ*M* and 1 m*M* hydrogen peroxide on reduced pyridine nucleotides was measured in liver microsomes from untreated control mice with fluorimetric detection of NADPH/NADH, and was found to be significantly decreased (a representative trace out of five is shown).

homogenate was not observed (data not shown). The oxidation of the intraluminal thioredoxin-motif containing oxidoreductases could be observed on immunoblots by using AMS labeling. The slower migrating reduced and the faster migrating oxidized form of ERp72 are clearly distinguishable on the blot; gulonolactone treatment resulted in a marked decrease in the reduced form (Fig. 4B). ERp72 might also be present in higher molecular weight disulfides with other proteins; however, they could not be visualized on the blots. In case of ERp46 a redox shift could be observed due to their oxidation upon gulonolactone treatment (Fig. 4C). DTT coadministration counteracted the effect of gulonolactone treatment on the redox state of these proteins. Immunoblotting of ERp72, ERp46, and ERp5 on nonreducing gels showed a faster migration of ERp46 in samples from gulonolactone-treated mice, while in case of the other two proteins the nonreducing gel did not reveal the difference in their redox state (Fig. 4D).

These acute alterations could not be detected in 12-h samples (Supplementary Fig. S3.), in accordance with our previous findings in 24-h samples (25).

The altered redox state of the ER lumen was accompanied by an early sign of ER stress (*i.e.*, the phosphorylation of eIF2α) (Fig. 4E). XBP1 splicing was instead observed in DTT-treated mice (Fig. 4F). Both changes were fully or partially reverted by the coadministration of the two substances (DTT and gulonolactone), indicating the ability of one to antagonize the effect of the other. No signs of ER stress were observed in the 12-h samples (Fig. S3.); moreover, the expression of ER chaperones PDI, Grp78, and Grp94 was not changed by any treatments, measured in either 30-min or 12-h samples (Figs. 4E and S3B).

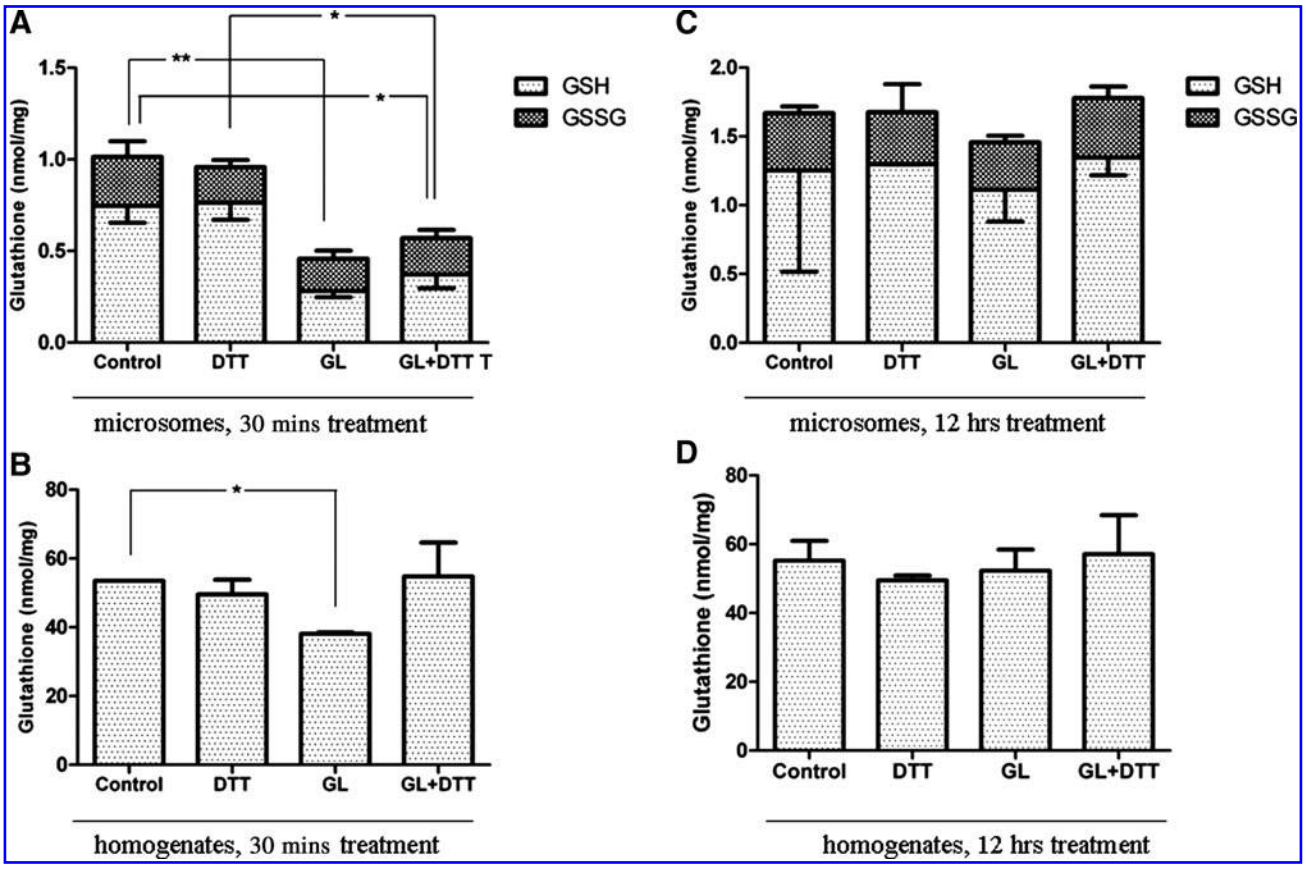

FIG. 3. Luminally produced H_2O_2 preferentially oxidizes microsomal glutathione. Mice treated with a single dose of gulonolactone (GL), dithiothreitol (DTT), or both (GL + DTT) were sacrificed 30 min **(A** and **B)** or 12 h **(C** and **D)** after the treatment. Total liver homogenates and liver microsomes were prepared and their glutathione contents were analyzed by HPLC. **(A)** Gulonolactone treatment resulted in a marked decrease in microsomal GSH content, while GSSG content remained unaffected. **(B)** Gulonolactone treatment moderately decreased the GSH content in liver homogenate. **(C, D)** 12 h after the treatment glutathione levels returned to the control values both in the microsomal fractions and in the homogenates. Results are expressed as nmoles/mg microsomal protein, mean ± S.D., $n = 3$-5, $^{**}p < 0.01$, $^{*}p < 0.05$.

ER-targeted hydrogen peroxide elimination interferes with oxidative folding

Cell lines devoted to secreting abundant amounts of disulfide-containing proteins (27) were prevented from reutilizing the intraluminal H_2O_2 produced during active oxidative folding with the expression of ER-targeted antioxidant enzyme catalase. As a control, a catalase mutant (Y358F-catalase) was also directed to the luminal compartment; the presence of tyrosine in the 358 position is crucial for the activity (32). The expression of ER-catalase and its mutant form was controlled in HEK293 cells (Fig. 5A) and the ER localization was verified with immunofluorescence microscopy (Fig. 5B). Both versions of catalase remained co-localized with ER-markers calreticulin, and did not co-localize with ERGIC-53; thus it was retained in the ER lumen and did not appear in the early secretory compartments.

Multimeric glycoproteins (*e.g.*, IgM) undergo a structural maturation in the ER until the fully assembled polymer —containing hundreds of disulfides —is released (7). When expressed in HEK293 cells, μ- and λ-chains of IgM experience polymerization and form disulfide-linked polymers, dimers, and monomers, until the mature immunoglobulin and —due to imperfect quality control mechanisms with respect to designated antibody secreting cells —some dimers are secreted into the medium (9). Antibody secretion of HEK293 cells were analyzed and compared with immunoblot after co-transfecting IgM components with wild- type or mutant ER-targeted catalase. We found that cells expressing ER-targeted catalase secreted less IgM polymers than mock-transfected cells; densitometric analysis showed a significantly decreased polymer/dimer ratio in the medium of ER-catalase-containing cells. The ER-targeted catalase expressing cells showed a decreased intracellular level of assembled polymers and a slightly increased amount of nonassembled intermediates (Figs. 5C and 5D). Cells expressing mutant catalase in the ER did not exhibit significant alteration either in polymer secretion or in intracellular assembly intermediates (data not shown).

The effect of H_2O_2 elimination on IgM assembly was also investigated in I29μ^+ lymphocytic cells. To investigate consequences of capturing immediately the ER-derived H_2O_2, I29μ^+ cells expressing ER-targeted catalase and its mutant version were created by stable transfection with lentiviral vectors. Plasma cells, being designated secretors, released

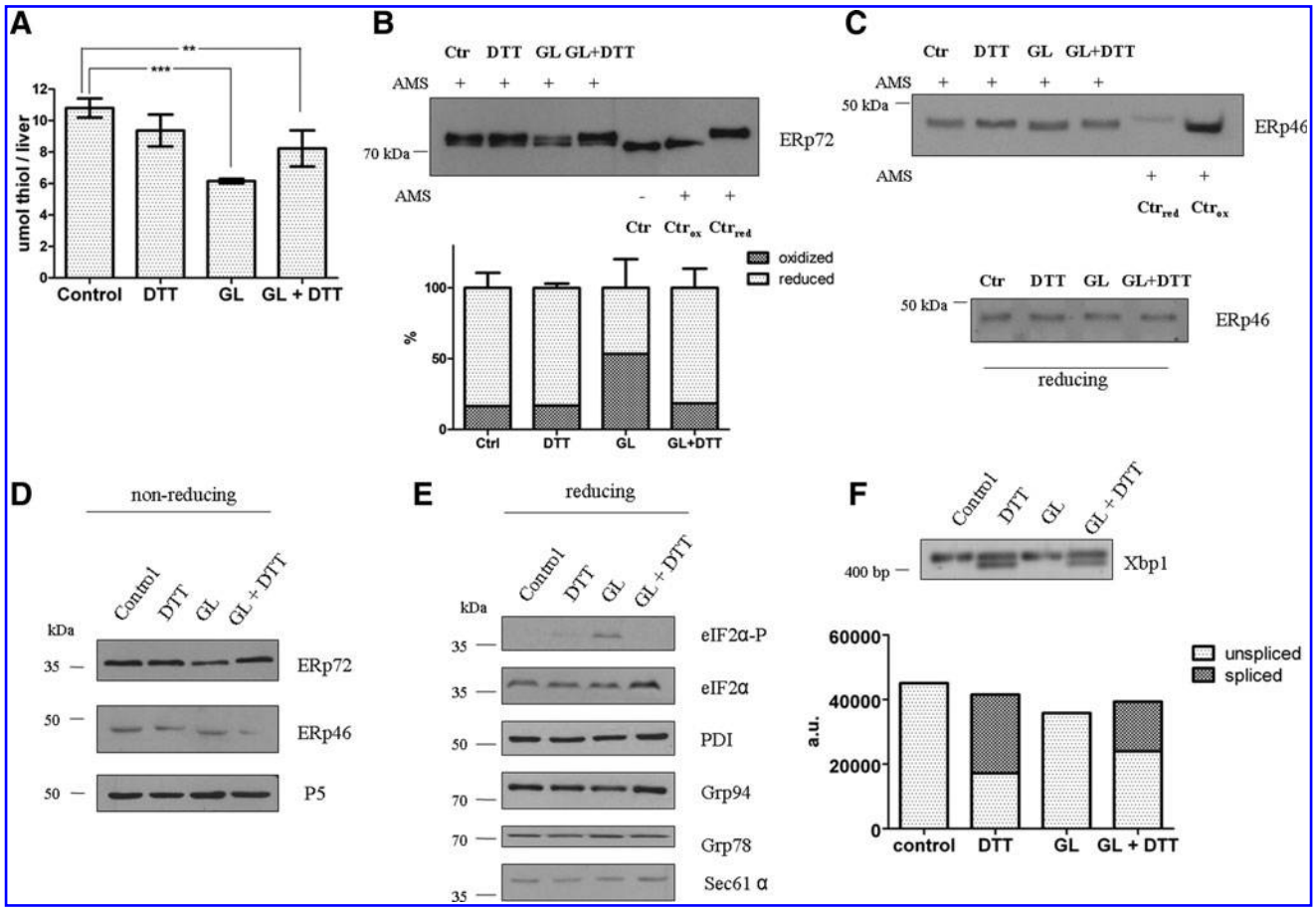

FIG. 4. Luminally produced H_2O_2 oxidizes microsomal protein thiols and provokes a mild ER stress. Mice treated with gulonolactone (GL), dithiothreitol (DTT), or both (GL + DTT) for 30 min, were sacrificed, and liver microsomes were isolated and analyzed. **(A)** A significant oxidation of protein thiols was observed in samples from GL-treated mice. DTT treatment reversed this effect. Results are expressed as mean ± S.D., $n = 4$–6, $^{***}p < 0.001$, $^{**}p < 0.01$. **(B)** The redox state of ERp72 was revealed by AMS labeling and consecutive immunoblot (*upper panel*). ERp72 appeared in both reduced and oxidized forms being more abundant its reduced form (*upper band*), while GL treatment equalized the ratio between the reduced (*upper band*) and oxidized (*lower band*) forms of the protein. Simultaneous DTT treatment set back the normal redox state of the protein. Reduced and oxidized controls were prepared from control mouse liver microsomes by treating them with the thiol-reducing agent DTT or the thiol-oxidizing agent diamide, respectively, prior to AMS labeling. Densitometric quantification of the gels (*lower panel*) confirmed the oxidizing effect of gulonolactone treatment. The abundance of oxidized and reduced forms is expressed as the percentage of total ERp72 in the corresponding lane. Results are expressed as mean ± S.D., $n = 4$. **(C)** The redox state of ERp46 (*upper panel*) was revealed by AMS labeling and consecutive immunoblot. A redox shift was observed due to the faster migration of the oxidized form of this protein upon gulonolactone treatment. *Lower panel* shows an immunoblot of Erp46 under reducing conditions, indicating no difference in the migration. Representative blots out of four and three are shown. **(D)** Immunoblot analysis of ERp72, ERp46, and ERp5 on nonreducing gel. A marked shift was observed in case of ERp46 in microsomes from GL-treated mice. A representative blot out of four is shown. **(E)** Immunoblot analysis showed that the phosphorylation of eIF2α appeared in GL treated animals, and was reversed by DTT treatment, while the expression level of different ER chaperons and foldases (PDI, Grp94, Grp78) remained unchanged. Sec61α was also detected as a loading control. **(F)** Splicing of XBP1 transcription factor occurred in DTT-treated animals. The concomitant GL treatment partially reversed the stressor effect of the reductant. Unspliced (*upper band*) and spliced (*lower band*) XBP1 cDNA were run on 2% agarose gel *(upper panel)* and quantified with densitometric analysis *(lower panel)*. Results were statistically different between DTT and GL + DTT treatments ($p < 0.05$). The figure shows a typical gel and its densitometric analysis.

only IgM polymers and not any assembly intermediates. Polymer secretion significantly decreased in those lines where H_2O_2 was captured within the lumen (Fig. 6A). Cell lysates derived from ER-catalase transfected I29μ^+ cells contained less IgM polymers as well, alike to the data obtained on the secreted material. Polymer assembly was also checked in I29μ^+ cells transfected with the mutant catalase, and was found to be not significantly different from controls (Fig. 6B). Decreased polymer secretion was not due to an increased cell death (Fig. 6C), as assessed by propidium iodide staining.

Discussion

Hydrogen peroxide, the side-product of oxidative protein folding, is an effective electron acceptor. On the basis of its pro-oxidant behavior, it has been supposed that enhanced

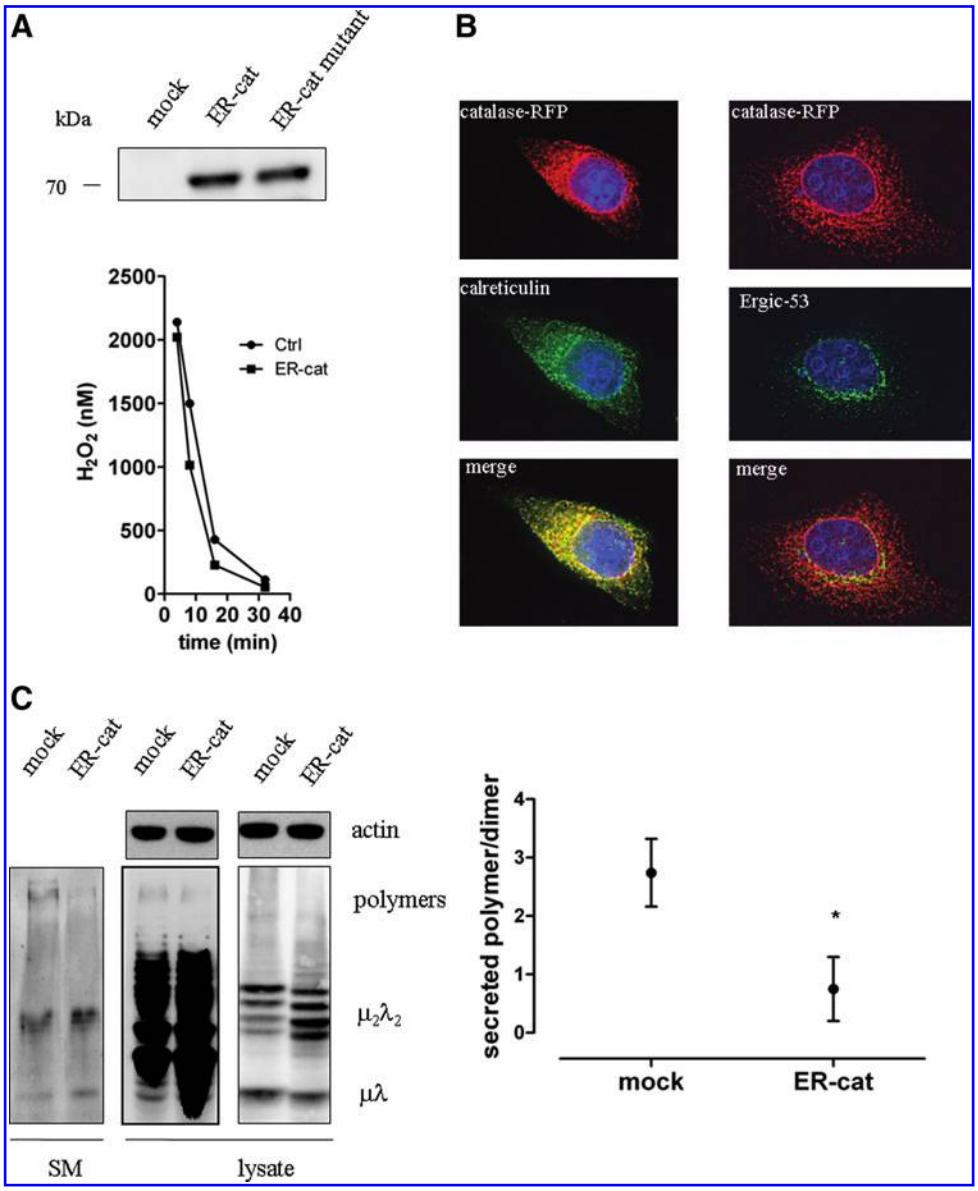

FIG. 5. ER-targeted catalase expression interferes with oxidative folding of immunoglobulin polymers in HEK293 cells. **(A)** ER-targeted catalase enzyme and its mutant variant were expressed in HEK293 cells and their expression was checked by immunoblotting in cell lysates (*upper panel*). The *lower panel* shows the time course of elimination of exogenously added hydrogen peroxide (100 μM) in control and ER-targeted catalase expressing cells. **(B)** Localization of ER-targeted catalase was controlled with fluorescence microscopy. Panels show a representative cell with nuclear staining [DAPI (4′,6-diamidino-2-phenylindole)], immunostaining of calreticulin or Ergic-53, and RFP-tagged ER-catalase along with composite images, whereas RFP-tagged ER catalase showed strong co-localization with the ER marker calreticulin, did not appear in the secretory compartment Ergic and was retained in the ER. **(C)** Analysis of secreted (SM) and intracellular (lysate) antibody polymers/assembly intermediates was performed with immunoblotting in HEK293 cells co-transfected with ER-targeted catalase and immunoglobulin subunits. A typical Western blots using antibodies to the heavy chain of IgM on secretory media and cell lysates (with longer and shorter exposition time) is shown. As loading control, cell lysates were immunoblotted against β-actin. Quantification of secreted immunoglobulin subunits by densitometric analysis of immunoblots revealed a lower polymer/dimer ratio in ER-catalase transfected cells comparing to the mock transfected ones. Results are expressed as mean ± S.D., $n = 4$, $^*P < 0.05$.

oxidative folding represents an oxidative burden in designated secretory cells. However, hydrogen peroxide as an alternative electron acceptor can also promote disulfide bond formation. Indeed, H_2O_2 *in vitro* was able to promote oxidative folding, resulting in the efficient formation of a natively folded protein containing proper disulfide bonds. The recent identification of ER peroxidases (PRDX4, GPx7, and GPx8) as PDI oxidants further strengthened the view that hydrogen peroxide can be productively used in oxidative folding.

The results obtained *in vivo* and reported here demonstrate that hydrogen peroxide contributes to the process of disulfide bond formation; its removal rather than its generation can

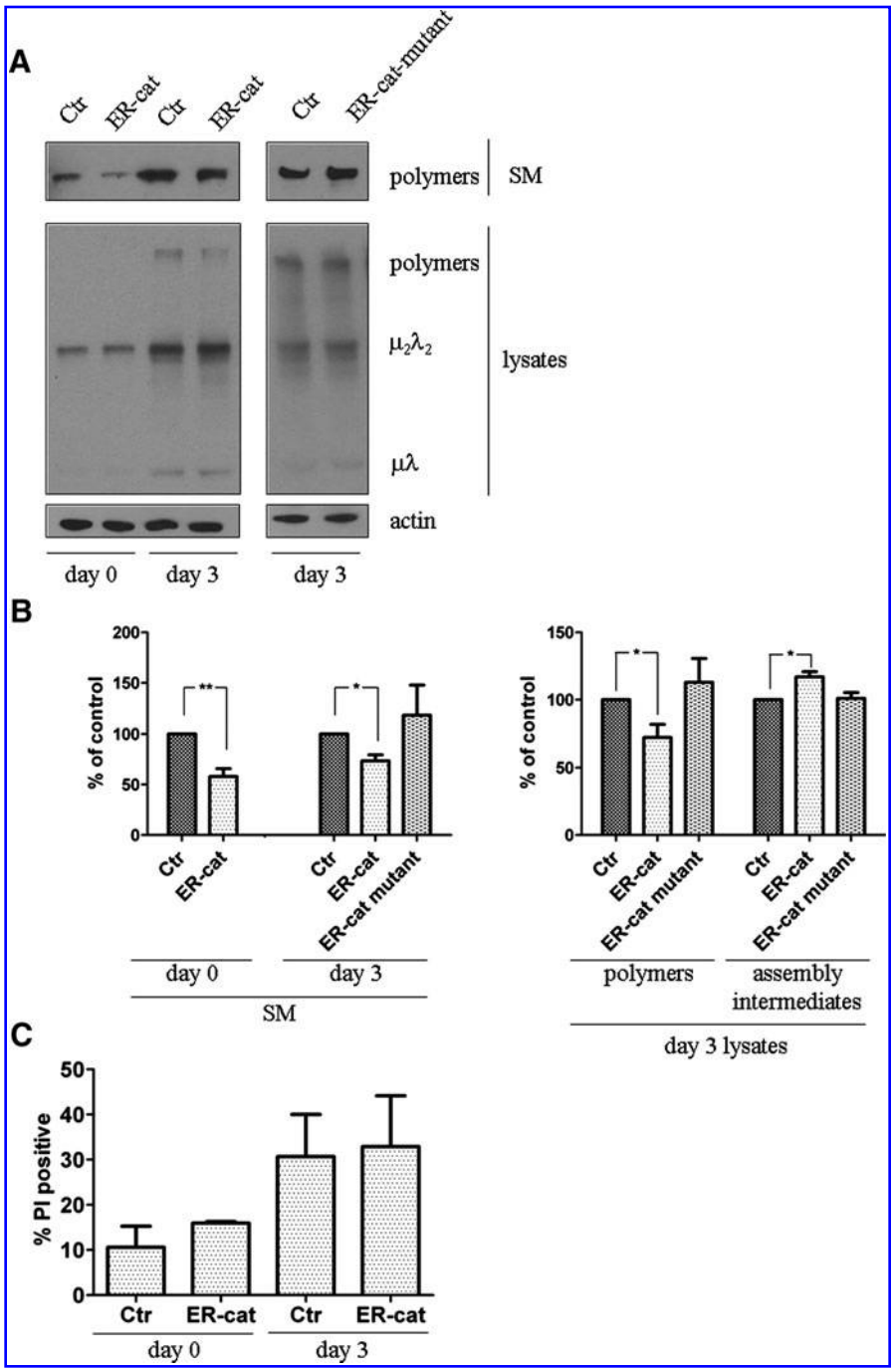

FIG. 6. ER-targeted catalase expression interferes with oxidative folding of immunoglobulin polymers in lymphocytic cells. (A) Western blots from undifferentiated (day 0) and differentiated (day 3) plasma cell lysates *(lower panel)* and secretory media (SM, *upper panel*) using antibodies to the heavy chain of IgM showed a decreased assembly and secretion of the polymers in cells expressing ER-targeted catalase (ER-cat) comparing to the mock-transfected control. Polymer assembly was not affected by the expression of mutant ER-cat. As loading control, cell lysates were immunoblotted against β-actin. A representative image out of three experiments is shown. **(B)** Densitometric analysis of three experiments, out of which a representative one is shown in **(A)**. *Left panel* shows the the result of the analysis of secreted polymers on day 0 and 3. *Right panel* shows the result of the analysis of intracellular polymers and assembly intermediates in lysates on day 3. Data are expressed as percentages of the control. Results are expressed as mean ± S.D., $n = 3$, $^{**}p < 0.01$, $^{*}p < 0.05$. **(C)** The expression of the ER-cat did not result in a decreased viability, as it was demonstrated by propidium iodide staining. Results are expressed as mean ± S.D., $n = 3$.

hinder the oxidative folding. ER-targeted overproduction of hydrogen peroxide, by the exogenous substrate supply of the ER resident gulonolactone oxidase *in vivo* in mice resulted in decreased glutathione and protein thiol content in the ER of the liver (Figs. 3A and 4A) and in a redox shift of ER oxidoreductases towards the oxidized direction (Figs. 4B and 4C). On the contrary, the stimulated decomposition of ER luminal hydrogen peroxide by the ER-targeted overexpression of catalase resulted in an impaired secretion of IgM in HEK293 (Fig. 5C) and I29μ^+ cells (Fig. 6A).

Manipulation of luminal hydrogen peroxide levels however was not accompanied with altered viability either *in vivo* or in the cellular models, indicating the robustness of ER redox control. Gulonolactone administration, although resulting in an acute, dramatic liver swelling and dilation of ER cisternae (Fig. 1) due to a temporary change of the permeability of the ER membrane (25), provoked only minor signs of ER stress; a transient increase in eIF2α phosphorylation was observed that was not accompanied with XBP1 activation or chaperon induction (Figs. 4D–4F). Thus, it can be supposed that altered proteostasis rather than redox imbalance is the main factor of ER stress upon protein overproduction.

ER-targeted hydrogen peroxide overproduction compromised not only the thiol/disulfide, but also the pyridine nucleotide redox system. Consumption of luminal NADPH was detected on the basis of microsomal cortisone-to-cortisol conversion and was verified directly in liver microsomes by hydrogen peroxide addition. The biochemical basis of this

phenomenon needs further studies. GSSG-mediated NADPH oxidation is not probable, due to the absence of glutathione reductase in the compartment (30). A peroxiredoxin-mediated pathway nevertheless can be taken into account (17). Moreover, the difference in the protective effect of DTT supplies a further proof for the uncoupling of the thiol–disulfide and the pyridine nucleotide redox systems. DTT co-administered with gulonolactone prevented liver swelling, morphological alterations, protein thiol oxidation, ERp72 redox shift, and eIF2α phosphorylation (*i.e.,* the effects presumably mediated by the oxidation of protein thiols), but did not counterbalance the altered redox state of pyridine nucleotides. Although the antagonistic effect of gulonolactone and DTT can be explained by their opposite redox effects, the different profile in the activation of the signaling pathways of ER stress needs further studies. However, several findings confirm the selective activation and divergent role of ER stress signaling pathways (21, 26, 33).

While hydrogen peroxide generation in the ER stimulated the oxidation of microsomal protein thiols in our *in vivo* model, the stimulated decomposition of ER luminal hydrogen peroxide by the ER-targeted overexpression of catalase resulted in an impaired secretion of IgM in cellular models (Figs. 5 and 6.). However, the vast majority of disulfide bonds necessary to fold $\mu 2\lambda 2$ intermediates are formed also in cells expressing active catalase. Only those mediating the polymerization or the retention of immature intermediates seem to be impaired; the subtle effect of lower levels of hydrogen peroxide on IgM polymerization suggests that further compartmentation or biochemical circuits are at work to assist the biogenesis of the complex molecule. The decreased secretion of IgM polymers and increased retention of assembly intermediates also suggest the significant contribution of quality control mechanisms, which are presumably activated by the impaired disulfide bond formation. The decreased IgM secretion and the activation of the quality control however cannot be merely attributed to the luminal overexpression of a protein, since the catalase mutant did not produce the same effects.

The results confirm the assumption that local oxidases other than Ero1 can contribute to the functioning of oxidative folding by providing hydrogen peroxide. Gulonolactone oxidase, however, cannot be regarded as a general hydrogen peroxide supplier; the enzyme is expressed usually only in the liver and in some species— including primates and guinea pig— is even absent. Apart from this aspect, hydrogen peroxide produced in the ER can be efficiently channeled into the electron transfer chain of oxidative protein folding, by using multiple routes involving ascorbate, PDI peroxidases, peroxiredoxins, or other electron carriers to be identified.

Materials and Methods

Materials

L-Gulono-γ-lactone, 5,5′-dithio-bis(2-nitrobenzoic acid), α,α'-dipyridyl, ascorbate, dithiothreitol, diamide, cortisone, cortisol, NADPH, MOPS, hexadimethrine bromide, lipopolysaccharides, and hydrogen peroxide were obtained from Sigma Chemical Co (St. Louis, MO).

Animal experiments

Male CD-1 mice (20–25 g body weight) and male Hartley guinea pigs (250–300 g body weight) were purchased from Charles River Hungary (Isaszeg). Animal treatments were approved by the Committee on Animal Experiments of Semmelweis University, Budapest. Animals were kept with *ad libitum* access to food and water. Gulonolactone (3.5 g/kg body weight) and dithiothreitol (150 mg/kg body weight) were dissolved in physiological saline and was injected intraperitoneally in a volume of 1 ml (in mice) or 10 ml (in guinea pigs). Control animals received an equivalent volume of the vehicle. Treatments with different agents were tolerated well by the animals. At various time points after treatment (0.5 or 12 h) animals were sacrificed. Liver samples were taken and processed for electron microscopy and for RNA isolation. The remnant of the liver was homogenized in sucrose–HEPES buffer (0.3 *M* sucrose, 0.02 *M* HEPES, pH 7.2) with a glass-Teflon homogenizer. The microsomal fraction was then isolated using fractional centrifugation as detailed elsewhere (23). Microsomes were resuspended in a KCl- MOPS buffer (100 m*M* KCl, 20 m*M* NaCl, 1 m*M* MgCl2, 20 m*M* MOPS, pH 7.2), were immediately frozen in liquid nitrogen, and kept in liquid nitrogen until use. The integrity of the microsomal membranes was assessed by using the mannose-6-phosphatase assay (6) and by measuring *p*-nitrophenol glucuronidation (15), which showed latency greater than 95%.

Electron microscopy

For transmission electron microscopy investigation, upon dissection after an *in vivo* treatment, the liver samples were immediately fixed in 0.5% glutaraldehyde + 2% paraformaldehyde (PolySciences Europe GmbH., Eppelheim, Germany) in 0.1 *M* cacodylate buffer (pH 7.2) containing 0.25 *M* sucrose and 2 m*M* $CaCl_2$ for 2 h at room temperature, then washed in 0.1 *M* cacodylate buffer. After postfixation in 1% osmium tetroxide (Serva Feinbiochemica GmbH., Heidelberg, Germany) in 0.1 *M* cacodylate buffer, liver samples were dehydrated in ascending series of ethanol, infiltrated in propylene oxide, and embedded in Durcupan ACM resin (Fluka AG, Buchs, Switzerland). Ultrathin sections were contrasted with uranyl acetate and lead citrate and electron micrographs were taken by a Jeol JEM1011 electron microscope operating at 60 kV.

Immunoblotting, antibodies

The protein concentration of samples was measured using the Bradford protein assay (Fermentas, Hanover, MD). Equal amounts of microsomal proteins (25–100 μg) were separated in SDS–PAGE and transferred to nitrocellulose filter membranes (Bio-Rad, Hercules, CA) by electroblotting. The filter membranes were incubated overnight with the primary antibodies (anti-eIF2α and anti-phospho-eIF2α are from Cell Signaling Technology, anti-ERp72 is from Calbiochem; sec61α, PDI, GRp78, GRp94, and H6PDH are from Santa Cruz Biotechnology; 11βHSD1 is from Cayman Chemical), and for 1 h with the species-specific peroxidase-conjugated secondary antibodies (anti-goat, anti-mouse, and anti-rabbit IgGs from Santa Cruz Biotechnology). The anti-myc murine monoclonal antibody 9E10 (8) was used to detect tagged proteins. The antibodies were detected using a chemiluminescence reagent (ECL) kit (Pierce, Rockford, IL) and blue-sensitive X-ray film. Equal protein loading was also verified by Ponceau-staining of the membrane and by β-actin detection. Band intensities were quantified by densitometry using Image Quant 5.2 software (Molecular Dynamic, Sunnyvale, CA). The thiol

redox state of ER foldases was investigated by alkylation with 4-acetamido-4′-maleimidylstilbene-2,2′-disulfonic acid (AMS; Molecular Probes–Invitrogen, Eugene, OR) as reported in (14). 200 μg microsomal proteins were precipitated with 5% trichloroacetic acid, washed two times with 70% acetone and two times with 0.1 *M* Tris buffer (pH 7.2). The resuspended proteins were reacted with 20 m*M* AMS for 15 min on ice, then for 15 min at 37°C. For the reduced and oxidized controls, microsomal samples from the liver of control mice corresponding to 200 μg protein were incubated at 37°C for 15 min with 50 m*M* dithiothreitol or with 25 m*M* diamide, respectively.

Analysis of XBP1 splicing

The splicing of XBP1 mRNA was analyzed as described by Yoshida *et al.* (38) with the following primers: sense 5′ CCT TGTGGTTGAGAACCAGG 3′ and antisense 5′ AGGCTTGGT GTATACATGG 3′ obtained from Sigma-Aldrich Co.

Metabolite measurements

Ascorbate contents were measured in trichloroacetic acid-soluble supernatants of the total liver homogenates by the method of Omaye *et al.* (29), based on the reduction of Fe^{3+} with the oxidation of ascorbate and the subsequent determination of the Fe^{2+}-α,α'-dipyridyl complex. The results were controlled by measuring the ascorbate contents with HPLC (40); these measurements confirmed the data gained by the dipyridyl method. Protein thiols were measured in the washed and resuspended pellets by the Ellman method (11) (Supplementary Fig. S4). Determination of glutathione content of liver or microsomes were performed by HPLC analysis as described earlier (25). Glutathione measurement from freeze–thawed microsomes gives a good approximation of the original ER glutathione levels because permeation of both GSH and GSSG through microsomal membranes is relatively slow. Hydrogen peroxide content of cellular supernatants was measured by Amplex® Red Assay Kit (Invitrogen, Carlsbad, CA) according to the manufacturer's instruction.

Measurement of cortisone–cortisol conversion

Microsomal cortisone–cortisol conversion (in both directions) was measured by incubating intact mouse liver microsomes (5 mg protein/ml) at 37°C in KCl/MOPS buffer in the presence of 10 μM cortisone or cortisol, respectively. Samples were incubated for 0, 5, 10, and 20 min, the reactions were terminated by adding ice-cold methanol. Samples were stored at −20°C until analysis. After sedimentation of the precipitates by centrifugation (20 000 *g* for 10 min at 4°C), the cortisol and cortisone content of the supernatants was measured by HPLC (Alliance 2690; Waters Corp., Milford, MA) using a Nucleosil 100 C18 column (5 μm 25×0.46) (Teknokroma). The eluent was 58% methanol, samples were eluted for 20 min and the absorbance was detected at 245 nm wavelength (Dual l Absorbance Detector 2487). The retention times of cortisol (approx. 13.5 min) and cortisone (approx. 15.5 min) were determined by injecting standards.

Fluorimetric detection of reduced pyridine nucleotides

Reduced pyridine nucleotides were detected based on their characteristic fluorescent spectrum in microsomes (30). Murine liver microsomal vesicles (1 mg/ml protein) from control mice were incubated in in KCl/MOPS buffer (pH 7.2) at 22°C. Fluorescence was monitored at 350 nm excitation and 460 nm emission wavelengths by using a Cary Eclipse fluorescence spectrophotometer (Varian). The activity of 11βHSD1 and H6PDH was measured on the basis of NADPH formation, as described earlier (2, 30).

Cell lines and culturing

HEK293 were grown in α-minimal essential medium (Invitrogen, Carlsbad, CA) supplemented with 10% fetal calf serum (FCS) at 37°C, 5% CO_2. The mouse B lymphoma cell line I29μ^+ cells were cultured in RPMI media (Invitrogen) supplemented with 10% defined FBS (HyClone Lab.), glutamax (1 m*M*), penicillin (100 U/ml), and streptomycin (100 μg/ml), and activated with LPS as described earlier (37).

Cell lysis and secretion assay

Cells were lysed in 10 m*M* Tris-HCl (pH 7.4), 150 m*M* NaCl, and 1% NP40, plus freshly added protease inhibitors (Roche, Basel, CH), and 10 m*M* *N*-ethylmaleimide (19) (Sigma Chemical Co), then centrifuged 15 min at 4°C 20,000 *g* to pellet nuclei. For secretion assay, HEK293 cells or differentiating I29μ^+ cells were washed twice in phosphate-buffered saline and cultured in OptiMem Medium (Invitrogen) in the absence of FCS for 4 h at a cell density of 1×10^6/ml. After centrifugation, spent media were supplemented with protease inhibitors and 10 m*M* NEM and analyzed. To detect IgM assembly intermediates, total cell lysates and cell supernatants were separated on NuPAGE 4-12% Bis-Tris gel (Invitrogen) and IgM intermediates were detected with polyclonal rabbit anti-mouse IgM from ZYMED (San Francisco, CA).

Vectors, cell transfections

Vectors encoding μ -chain and λ –chain were described earlier. The pCMV-myc-ER expression vectors (Invitrogen V823-20) encoding catalase, catalase-RFP, catalase-Y358F, and catalase-Y358F-RFP were kind gifts of M. Geiszt (Semmelweis University, Dept. of Physiology, Budapest, Hungary). The inserts were amplified with the primers sense 5′ CGTGTACGGTGGGAGGTCTA 3′ and antisense 5′ AGG CACAGTCGAGGCTGAT 3′ and were introduced with Sal I./Sma I. sites into a bidirectional lentiviral vector #945 (which was a kind gift of L. Naldini, Vita Salute San Raffaele University, Milan, Italy) expressing GFP in one direction and the introduced sequence in the other. Cloning was performed with StrataClone PCR cloning kit (Stratagene, La Jolla, CA). Virus packaging and cell infection was performed according to Follenzi *et al.* (13). Transfected I29 μ^+ cells were selected on the basis of GFP expression. HEK-293 cells were transiently transfected with a solution of polyethyleneimine "MAX" linear MW 25000, (Polysciences, Inc, Warrington, PA), plasmid DNA, and PBS. The mix solution was incubated for 20 min at RT before addition to cultured cells for 6 hours.

Immunofluorescence

HEK293 cells were grown directly (and, when indicated, transiently transfected) on 10 mm^2 cover-slips, were fixed in 3% paraformaldehyde and permeabilized with 0.1% Triton×

100. After decoration with the indicated antibodies—rabbit anti-calreticulin was from Stressgen (Victoria, BC Canada), Alexa Fluor 488 goat anti-rabbit IgG (H+L) was from Molecular Probes—cells were stained with Hoechst (Molecular Probes), and then samples werepreprared in Mowiol.

Flow cytometry

About 1×10^6 differentiating B cells were washed in phosphate-buffered saline/0.5% bovine serum albumin, and cell death rate was assessed by propidium iodide (PI) staining following the manufacturer's instructions (BD Bioscience, San Jose, CA). After extensive washing, samples were analyzed by FACSCalibur and data were analyzed by the CellQuestPRO (BD Bioscience) or FCS Express (De Novo Software, Los Angeles, CA) software.

Statistical analysis

The quantified results are shown as mean values ± S.D. Statistical analysis for enzyme activities was performed with one-way ANOVA followed by the Tukey–Kramer Multiple Comparison Test (GraphPad InStat).

Acknowledgments

We thank Zsófia Kováts for skillful technical assistance in the electron microscopy work, Valéria Mile for expert technical assistance, M. Geiszt for the catalase plasmids and L. Naldini for the lentiviral vectors. This work was supported by the Hungarian Scientific Research Fund (OTKA NN 78300), by the János Bolyai Research Scholarship of the Hungarian Academy of Sciences (to ÉM), by the New Széchenyi Plan (TÁMOP-4.2.1./B-09/1/KMR-2010-0001) and by FEBS short term fellowhip (to ÉM). We thank AIRC (IG and 5x1000 program), Regione Lombardia (ASTIL program), and Telethon Italy (GGP06155). The acquisition of a JEOL JEM-1011 transmission electron microscope was supported by a grant of Széchenyi Plan (TÁMOP-4.2.1./B-09/1/KMR-2010-0003).

Author Disclosure Statement

No competing financial interests exist.

References

1. Appenzeller-Herzog C. Glutathione- and non-glutathione-based oxidant control in the endoplasmic reticulum. *J Cell Sci* 124: 847–855, 2011.
2. Banhegyi G, Benedetti A, Fulceri R, and Senesi S. Cooperativity between 11beta-hydroxysteroid dehydrogenase type 1 and hexose-6-phosphate dehydrogenase in the lumen of the endoplasmic reticulum. *J Biol Chem* 279: 27017–27021, 2004.
3. Banhegyi G, Csala M, Braun L, Garzo T, and Mandl J. Ascorbate synthesis-dependent glutathione consumption in mouse liver. *FEBS Lett* 381: 39–41, 1996.
4. Bertolotti M, Yim SH, Garcia-Manteiga JM, Masciarelli S, Kim YJ, Kang MH, Iuchi Y, Fujii J, Vene R, Rubartelli A, Rhee SG, and Sitia R. B- to plasma-cell terminal differentiation entails oxidative stress and profound reshaping of the antioxidant responses. *Antioxid Redox Signal* 13: 1133–1144, 2010.
5. Bulleid NJ and Ellgaard L. Multiple ways to make disulfides. *Trends Biochem Sci*, 36: 485–492, 2011.
6. Burchell A, Hume R, and Burchell B. A new microtechnique for the analysis of the human hepatic microsomal glucose-6-phosphatase system. *Clin Chim Acta* 173: 183–191, 1988.
7. Cenci S, van Anken E, and Sitia R. Proteostenosis and plasma cell pathophysiology. *Curr Opin Cell Biol* 23: 216–222, 2011.
8. Chen TA and Allfrey VG. Rapid and reversible changes in nucleosome structure accompany the activation, repression, and superinduction of murine fibroblast protooncogenes c-fos and c-myc. *Proc Natl Acad Sci USA* 84: 5252–5256, 1987.
9. Cortini M and Sitia R. ERp44 and ERGIC-53 synergize in coupling efficiency and fidelity of IgM polymerization and secretion. *Traffic* 11: 651–659, 2010.
10. Dzyakanchuk AA, Balazs Z, Nashev LG, Amrein KE, and Odermatt A. 11beta-Hydroxysteroid dehydrogenase 1 reductase activity is dependent on a high ratio of NADPH/NADP(+) and is stimulated by extracellular glucose. *Mol Cell Endocrinol* 301: 137–141, 2009.
11. Ellman G and Lysko H. A precise method for the determination of whole blood and plasma sulfhydryl groups. *Anal Biochem* 93: 98–102, 1979.
12. Enyedi B, Varnai P, and Geiszt M. Redox state of the endoplasmic reticulum is controlled by Ero1L-alpha and intraluminal calcium. *Antioxid Redox Signal* 13: 721–729, 2010.
13. Follenzi A, Ailles LE, Bakovic S, Geuna M, and Naldini L. Gene transfer by lentiviral vectors is limited by nuclear translocation and rescued by HIV-1 pol sequences. *Nat Genet* 25: 217–222, 2000.
14. Frand AR and Kaiser CA. Two pairs of conserved cysteines are required for the oxidative activity of Ero1p in protein disulfide bond formation in the endoplasmic reticulum. *Mol Biol Cell* 11: 2833–2843, 2000.
15. Fulceri R, Banhegyi G, Gamberucci A, Giunti R, Mandl J, and Benedetti A. Evidence for the intraluminal positioning of p-nitrophenol UDP-glucuronosyltransferase activity in rat liver microsomal vesicles. *Arch Biochem Biophys* 309: 43–46, 1994.
16. Gross E, Sevier CS, Heldman N, Vitu E, Bentzur M, Kaiser CA, Thorpe C, and Fass D. Generating disulfides enzymatically: reaction products and electron acceptors of the endoplasmic reticulum thiol oxidase Ero1p. *Proc Natl Acad Sci USA* 103: 299–304, 2006.
17. Kalinina EV, Chernov NN, and Saprin AN. Involvement of thio-, peroxi-, and glutaredoxins in cellular redox-dependent processes. *Biochemistry (Mosc)* 73: 1493–1510, 2008.
18. Karala AR, Lappi AK, Saaranen MJ, and Ruddock LW. Efficient peroxide-mediated oxidative refolding of a protein at physiological pH and implications for oxidative folding in the endoplasmic reticulum. *Antioxid Redox Signal* 11: 963–970, 2009.
19. Kennedy DJ, Colyer WR, Brewster PS, Ankenbrandt M, Burket MW, Nemeth AS, Khuder SA, Thomas WJ, Shapiro JI, and Cooper CJ. Renal insufficiency as a predictor of adverse events and mortality after renal artery stent placement. *Am J Kidney Dis* 42: 926–935, 2003.
20. Kiuchi K, Nishikimi M, and Yagi K. Purification and characterization of L-gulonolactone oxidase from chicken kidney microsomes. *Biochemistry* 21: 5076–5082, 1982.
21. Ma Y, Shimizu Y, Mann MJ, Jin Y, and Hendershot LM. Plasma cell differentiation initiates a limited ER stress response by specifically suppressing the PERK-dependent branch of the unfolded protein response. *Cell Stress Chaperones* 15: 281–293, 2010.
22. Malhotra JD and Kaufman RJ. Endoplasmic reticulum stress and oxidative stress: A vicious cycle or a double-edged sword? *Antioxid Redox Signal* 9: 2277–2293, 2007.
23. Margittai E and Banhegyi G. Isocitrate dehydrogenase: A NADPH-generating enzyme in the lumen of the endoplasmic reticulum. *Arch Biochem Biophys* 471: 184–190, 2008.

24. Margittai E and Banhegyi G. Oxidative folding in the endoplasmic reticulum: towards a multiple oxidant hypothesis? *FEBS Lett* 584: 2995–2998, 2010.
25. Margittai E, Low P, Szarka A, Csala M, Benedetti A, and Banhegyi G. Intraluminal hydrogen peroxide induces a permeability change of the endoplasmic reticulum membrane. *FEBS Lett* 582: 4131–4136, 2008.
26. Masciarelli S, Fra AM, Pengo N, Bertolotti M, Cenci S, Fagioli C, Ron D, Hendershot LM, and Sitia R. CHOP-independent apoptosis and pathway-selective induction of the UPR in developing plasma cells. *Mol Immunol* 47: 1356–1365, 2010.
27. Masciarelli S and Sitia R. Building and operating an antibody factory: redox control during B to plasma cell terminal differentiation. *Biochim Biophys Acta* 1783: 578–588, 2008.
28. Nguyen VD, Saaranen MJ, Karala AR, Lappi AK, Wang L, Raykhel IB, Alanen HI, Salo KE, Wang CC, and Ruddock LW. Two endoplasmic reticulum PDI peroxidases increase the efficiency of the use of peroxide during disulfide bond formation. *J Mol Biol* 406: 503–515, 2011.
29. Omaye ST, Turnbull JD, and Sauberlich HE. Selected methods for the determination of ascorbic acid in animal cells, tissues, and fluids. *Methods Enzymol* 62: 3–11, 1979.
30. Piccirella S, Czegle I, Lizak B, Margittai E, Senesi S, Papp E, Csala M, Fulceri R, Csermely P, Mandl J, Benedetti A, and Banhegyi G. Uncoupled redox systems in the lumen of the endoplasmic reticulum. Pyridine nucleotides stay reduced in an oxidative environment. *J Biol Chem* 281: 4671–4677, 2006.
31. Puskas F, Braun L, Csala M, Kardon T, Marcolongo P, Benedetti A, Mandl J, and Banhegyi G. Gulonolactone oxidase activity-dependent intravesicular glutathione oxidation in rat liver microsomes. *FEBS Lett* 430: 293–296, 1998.
32. Putnam CD, Arvai AS, Bourne Y, and Tainer JA. Active and inhibited human catalase structures: Ligand and NADPH binding and catalytic mechanism. *J Mol Biol* 296: 295–309, 2000.
33. Schroder M and Kaufman RJ. Divergent roles of IRE1alpha and PERK in the unfolded protein response. *Curr Mol Med* 6: 5–36, 2006.
34. Senesi S, Csala M, Marcolongo P, Fulceri R, Mandl J, Banhegyi G, and Benedetti A. Hexose-6-phosphate dehydrogenase in the endoplasmic reticulum. *Biol Chem* 391: 1–8, 2010.
35. Tavender TJ, Springate JJ, and Bulleid NJ. Recycling of peroxiredoxin IV provides a novel pathway for disulphide formation in the endoplasmic reticulum. *EMBO J* 29: 4185–4197, 2010.
36. Tu BP and Weissman JS. The FAD- and O(2)-dependent reaction cycle of Ero1-mediated oxidative protein folding in the endoplasmic reticulum. *Mol Cell* 10: 983–994, 2002.
37. van Anken E, Romijn EP, Maggioni C, Mezghrani A, Sitia R, Braakman I, and Heck AJ. Sequential waves of functionally related proteins are expressed when B cells prepare for antibody secretion. *Immunity* 18: 243–253, 2003.
38. Yoshida H, Matsui T, Yamamoto A, Okada T, and Mori K. XBP1 mRNA is induced by ATF6 and spliced by IRE1 in response to ER stress to produce a highly active transcription factor. *Cell* 107: 881–891, 2001.
39. Zito E, Melo EP, Yang Y, Wahlander A, Neubert TA, and Ron D. Oxidative protein folding by an endoplasmic reticulum-localized peroxiredoxin. *Mol Cell* 40: 787–797, 2010.
40. Zsigmond L, Tomasskovics B, Deák V, Rigó G, Szabados L, Bánhegyi G, and Szarka A. Enhanced activity of galactono-1,4-lactone dehydrogenase and ascorbate-glutathione cycle in mitochondria from complex III deficient Arabidopsis. *Plant Physiol Biochem* 49: 809–815, 2011.

Address correspondence to:
Prof. Gábor Bánhegyi
Department of Medical Chemistry, Molecular Biology and Pathobiochemistry
POB 260
Semmelweis University
Budapest 1444
Hungary

E-mail: gabor.banhegyi@eok.sote.hu

Date of first submission to ARS Central, August 5, 2011; date of final revised submission, February 17, 2012; date of acceptance, February 22, 2012.

Abbreviations Used

11βHSD1 = 11β-hydroxysteroid dehydrogenase type 1
AMS = 4-acetamido-4′-maleimidylstilbene-2,2′-disulfonic acid
DTT = dithiothreitol
eIF2α = eukaryotic initiation factor 2 α
ER = endoplasmic reticulum
ERGIC-53 = endoplasmic reticulum golgi intermediate compartment 53
Ero1 = ER oxidoreductin 1
ERp72 = endoplasmic reticulum protein 72
GL = gulonolactone
GPx = glutathione peroxidase
Grp78/94 = glucose regulated protein 78/94
GSH = reduced glutathione
GSSG = oxidized glutathione
H_2O_2 = hydrogen peroxide
H6PDH = hexose-6-phosphate dehydrogenase
NAD(P) = nicotinamide adenine dinucleotide (phosphate)
NEM = N-ethyl maleimide
PDI = protein disulfide isomerase
PRDX4 = peroxiredoxin 4
XBP1 = X-box binding protein 1